THE EMBO JOURNAL

UCP2 regulates energy metabolism and differentiation potential of human pluripotent stem cells

Jin Zhang[1], Ivan Khvorostov[1], Jason S Hong[1], Yavuz Oktay[2], Laurent Vergnes[3], Esther Nuebel[2], Paulin N Wahjudi[4], Kiyoko Setoguchi[1], Geng Wang[2], Anna Do[1], Hea-Jin Jung[1], J Michael McCaffery[5], Irwin J Kurland[6], Karen Reue[3,7], Wai-Nang P Lee[4], Carla M Koehler[2,7,]* and Michael A Teitell[1,7,8,]*

[1]Department of Pathology and Laboratory Medicine, University of California, Los Angeles, CA, USA, [2]Department of Chemistry and Biochemistry, University of California, Los Angeles, CA, USA, [3]Department of Human Genetics, University of California, Los Angeles, CA, USA, [4]Department of Pediatrics, LA Biomedical Research Institute, Torrance, CA, USA, [5]Department of Biology, Integrated Imaging Center, Johns Hopkins University, Baltimore, MD, USA, [6]Department of Medicine, Stable Isotopes and Metabolomics Core Facility, Albert Einstein College of Medicine Diabetes Center, Bronx, NY, USA, [7]Molecular Biology Institute, University of California, Los Angeles, CA, USA and [8]Broad Stem Cell Research Center, Jonsson Comprehensive Cancer Center, Center for Cell Control, and California NanoSystems Institute, University of California, Los Angeles, CA, USA

It has been assumed, based largely on morphologic evidence, that human pluripotent stem cells (hPSCs) contain underdeveloped, bioenergetically inactive mitochondria. In contrast, differentiated cells harbour a branched mitochondrial network with oxidative phosphorylation as the main energy source. A role for mitochondria in hPSC bioenergetics and in cell differentiation therefore remains uncertain. Here, we show that hPSCs have functional respiratory complexes that are able to consume O_2 at maximal capacity. Despite this, ATP generation in hPSCs is mainly by glycolysis and ATP is consumed by the F_1F_0 ATP synthase to partially maintain hPSC mitochondrial membrane potential and cell viability. Uncoupling protein 2 (UCP2) plays a regulating role in hPSC energy metabolism by preventing mitochondrial glucose oxidation and facilitating glycolysis via a substrate shunting mechanism. With early differentiation, hPSC proliferation slows, energy metabolism decreases, and UCP2 is repressed, resulting in decreased glycolysis and maintained or increased mitochondrial glucose oxidation. Ectopic *UCP2* expression perturbs this metabolic transition and impairs hPSC differentiation. Overall, hPSCs contain active mitochondria and require *UCP2* repression for full differentiation potential.

*Corresponding author. CM Koehler, Department of Chemistry and Biochemistry, University of California, Los Angeles, 607 Charles E. Young Drive East, Los Angeles, CA 90095, USA. Tel.: +1 310 794 4834; Fax: +1 310 206 4038; E-mail: koehlerc@chem.ucla.edu or MA Teitell, Department of Pathology and Laboratory Medicine, University of California, 675 Charles E. Young Drive South, Los Angeles, CA 90095, USA. Tel.: +1 310 206 6754; Fax: +1 310 267 0382; E-mail: mteitell@mednet.ucla.edu

Introduction

A distinguishing feature of human pluripotent stem cells (hPSCs) compared with differentiated cells is the capacity for self-renewal to maintain pluripotency. Self-renewal is supported by unique chromatin modifications (Meshorer and Misteli, 2006) and a regulatory circuit comprised of OCT4, NANOG, and SOX2 transcription factors (Boyer et al, 2005). hPSCs proliferate relatively fast, with shortened cell cycle times and a higher proportion of cells in S phase compared with most differentiated cell types (Becker et al, 2006). Differences in energy status and biosynthesis from distinct physiologies also distinguish hPSCs from differentiated cells, although the extent and regulation of these differences is unknown. Thus, metabolism could provide a relatively unexplored distinguishing feature between hPSCs and differentiated cells.

Mitochondria are central organelles in carbohydrate, lipid, and amino-acid metabolism. Studies suggest that there are few, rounded, and non-fused mitochondria with underdeveloped cristae in human or mouse embryonic stem cells (ESCs) (St John et al, 2005; Cho et al, 2006; Chung et al, 2010; Prigione et al, 2010) Also, hPSCs produce more lactate than differentiated cells (Chung et al, 2010; Prigione et al, 2010), suggesting that glycolysis supercedes oxidative phosphorylation (OXPHOS) and that hPSC mitochondria may be metabolically inactive. However, this important assumption has not been thoroughly tested and it remains unclear how glycolysis and respiration contribute to the hPSC metabolic profile.

Uncoupling proteins (UCPs) are mitochondrial inner membrane proteins that regulate cell metabolism (Nicholls and Rial, 1999; Klingenberg and Echtay, 2001; Brand and Esteves, 2005). UCP1 mediates proton movement from the mitochondrial intermembrane space to the matrix, which uncouples electron transport from ATP synthesis in brown fat to generate heat (Klingenberg and Huang, 1999). In contrast, the function(s) of the widely expressed UCPs, including UCP2 and UCP3, are still controversial (Brand and Esteves, 2005; Bouillaud, 2009). UCP2 and UCP3 show uncoupling activity with *in vitro* proteoliposome assays (Echtay et al, 2001) or when activated by fatty acids and free radical-derived alkenals (Considine et al, 2003; Brand et al, 2004a, b). However, UCP2 and UCP3 have not shown physiological uncoupling activity (Cadenas et al, 2002; Couplan et al, 2002). Instead,
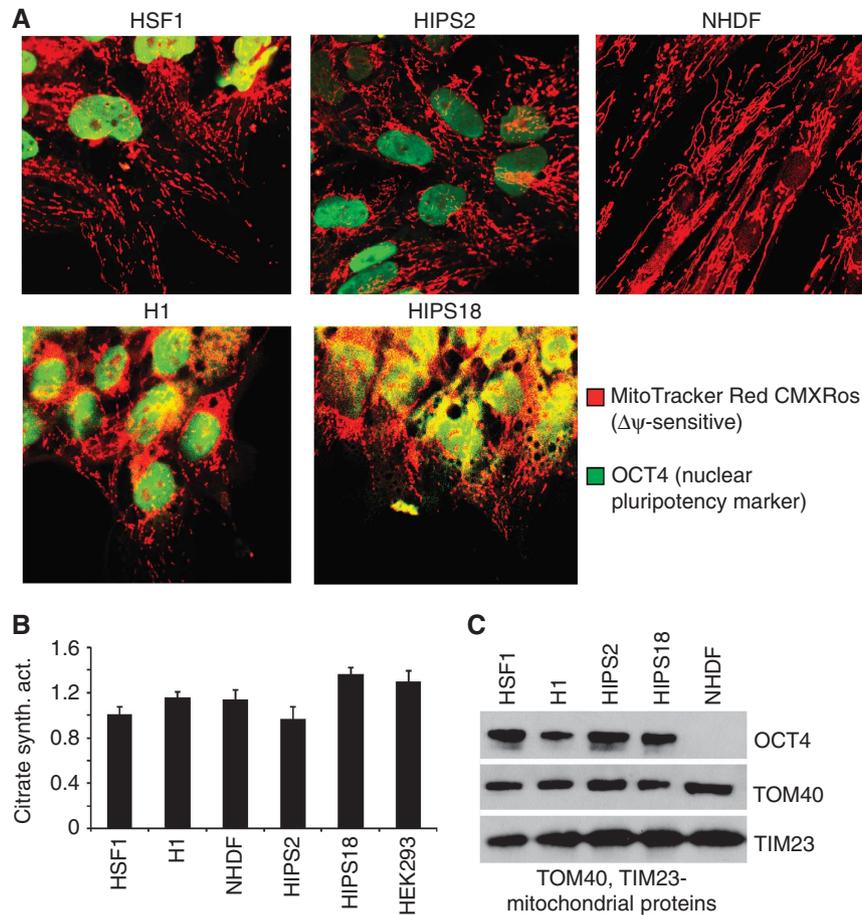
Figure 1 hPSC mitochondrial morphology and abundance. (**A**) A fragmented hPSC mitochondrial network is shown by confocal microscopy. (**B**) Ratio of citrate synthase enzyme activity to total cellular protein is plotted, normalized to 1.0 for HSF1. Data are expressed as mean ± s.d. ($n = 3$). (**C**) Representative western blot with 50 µg protein loaded per lane.

studies show that UCP2 augments fatty acid or glutamine oxidation and decreases glucose-derived pyruvate oxidation in mitochondria (Pecqueur *et al*, 2008, 2009; Bouillaud, 2009; Emre and Nubel, 2010). UCP2 blocking of pyruvate entry into the tricarboxylic acid (TCA) cycle has been postulated but not experimentally validated as a mechanism for enhancing aerobic glycolysis, consistent with UCP2 expression mainly in glycolytic tissues (Pecqueur *et al*, 2001) and in glycolysis-switched cancer cells (Pecqueur *et al*, 2001; Samudio *et al*, 2008, 2009; Ayyasamy *et al*, 2011). Therefore, UCP2 could be a gatekeeper for the oxidation of carbon substrates, such as glucose. Notably, no role has been described for UCPs in hPSC bioenergetics to date. Here, we evaluated bioenergetics in human ESCs (hESCs), human-induced pluripotent stem cells (hIPSCs), and differentiated cells. We report an important role for UCP2 in regulating hPSC energy metabolism and the fate of early differentiating hPSCs.

Results

A conserved mitochondrial mass ratio for hPSCs and differentiated cells

The distribution, abundance, fusion–fission status, and cristae structure of mitochondria regulates O_2 consumption, bioenergetics, apoptosis, and autophagy (Frank *et al*, 2001; Narendra *et al*, 2008; Chan *et al*, 2010; Sauvanet *et al*, 2010). Therefore, the morphology and abundance of hPSC and

fibroblast mitochondria were assessed for changes with differentiation or reprogramming. Confocal microscopy with MitoTracker Red CMXRos showed that the mitochondria in hESCs (HSF1 and H1 lines), and to a slightly lesser extent in hIPSCs (HIPS2 and HIPS18 lines), are punctate, or fragmented, compared with the well-developed filamentous network of normal human dermal fibroblasts (NHDFs, also called fibroblasts) (Figure 1A). hESCs differentiated by bFGF withdrawal also establish a filamentous mitochondrial network within days (Supplementary Figure S1A). Notably, hIPSC lines HIPS2 and HIPS18 were reprogrammed from NHDFs (Lowry *et al*, 2008), indicating that mitochondrial morphology is reversible with de-differentiation. Combined, the data show that mitochondrial fusion–fission and network morphology reflect the extent of cell differentiation.

The F_1F_0 ATP synthase appears to play a scaffolding role for the mitochondrial inner membrane cristae structure and impacts OXPHOS activity and cellular ATP levels (Giraud *et al*, 2002; Paumard *et al*, 2002; Minauro-Sanmiguel *et al*, 2005; Buzhynskyy *et al*, 2007; Campanella *et al*, 2008; Strauss *et al*, 2008). Therefore, the cristae structure of hPSCs was examined as a potential indicator of mitochondrial function. Transmission electron microscopy shows that hPSC cristae are swollen, circular, and disorganized compared with the linear, stacked cristae observed in many differentiated cell types, including fibroblasts (Supplementary Figure S1B). These features are similar to those seen in mouse ESCs and
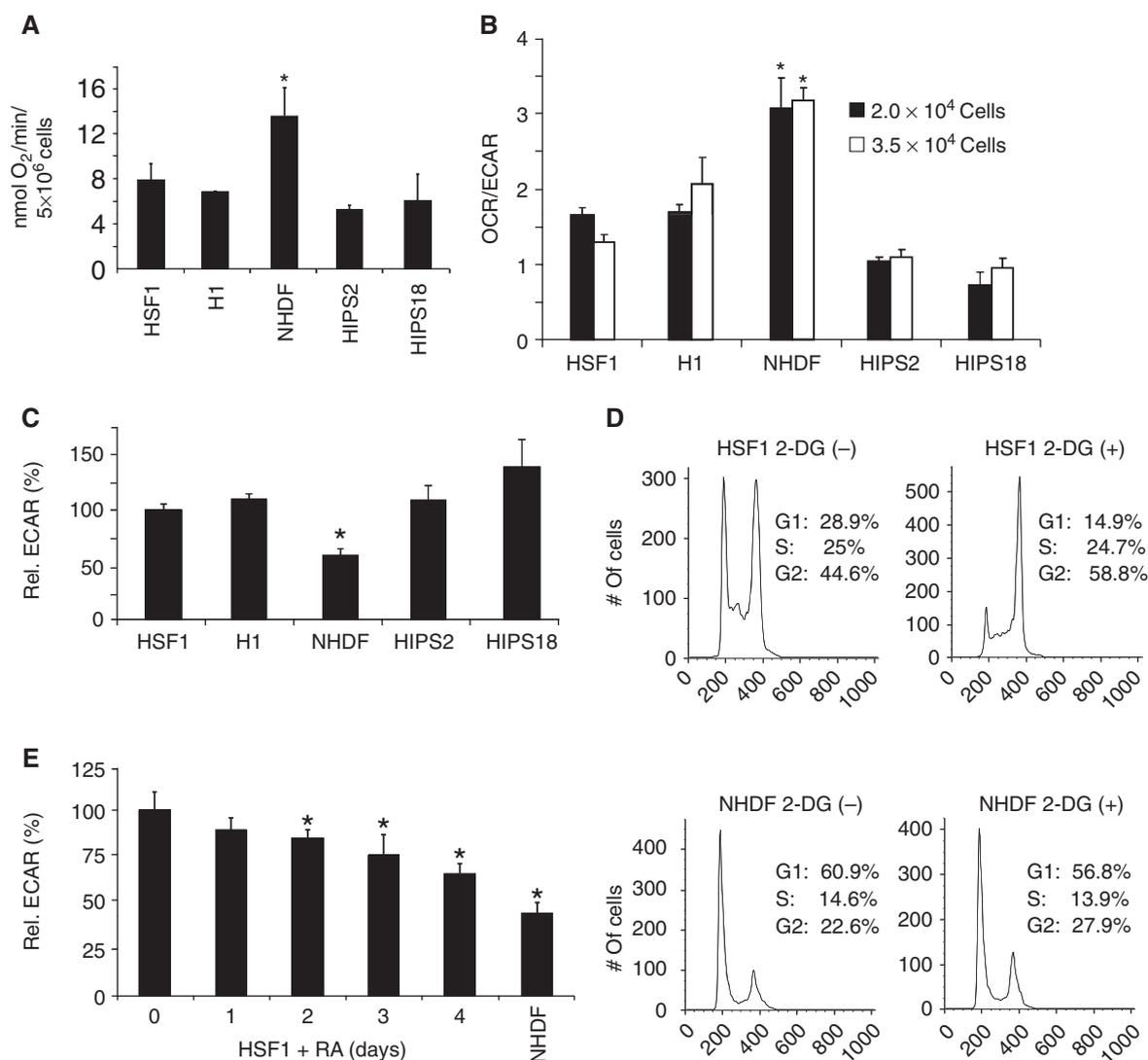
Figure 2 hPSCs consume O_2 and are programmed for glycolysis. (**A**) OCR in room air measured with a Clark-type O_2 electrode in intact cells. Data are expressed as mean ± s.d. ($n=3$), *$P<0.05$. (**B**) OCR to ECAR ratios measured by the XF24 extracellular flux analyser is shown. Data are expressed as mean ± s.d. ($n=3$), *$P<0.005$. (**C**) ECAR normalized to protein concentration is shown. Data are expressed as mean ± s.d. ($n=3$), *$P<0.05$. (**D**) Cells were incubated with 150 mM 2-DG for 45 min, followed by flow cytometry and cell-cycle profile analyses. (**E**) HSF1 cells were induced to differentiate by 10 μM RA for 4 days and ECAR determined. Data are expressed as mean ± s.d. ($n=3$), *$P<0.05$.

for a different set of hPSCs (Baharvand and Matthaei, 2003; Prigione *et al*, 2010). Less orderly cristae and a fragmented network suggests that PSC mitochondria are less functional than differentiated cell mitochondria.

Prior studies reported few mitochondria in hESCs (St John *et al*, 2005; Facucho-Oliveira *et al*, 2007). However, the ratio of mitochondrial to total cell protein mass is a more informative comparison between cell types and stages. Citrate synthase marks the mitochondrial matrix (Morgunov and Srere, 1998) and is commonly used as an indicator of mitochondrial function and mass. Citrate synthase enzymatic activity normalized to total protein is similar between hPSCs, hPSCs induced to differentiate by retinoic acid (RA) (Pan *et al*, 2007), and fibroblasts (Figure 1B; Supplementary Figure S1C). Also, the translocons of the inner (TIM23) and outer (TOM40) mitochondrial membranes accurately reflect mitochondrial mass and both are expressed at similar levels relative to the total protein content in hPSCs, RA-differentiated hPSCs, and fibroblasts (Figure 1C; Supplementary

Figure S1D). Fibroblast cell diameters are larger (~ 25–$35\,\mu m$) and cell volumes (assuming a spherical shape) are much larger ($\sim 16\,000\,\mu m^3$) than hPSCs (~ 15–$20\,\mu m$ and $\sim 3000\,\mu m^3$, respectively) (Supplementary Figure S1E). Fibroblasts also have 1.5- to 2-fold more protein than hPSCs, suggesting on a per cell basis there will be more mitochondrial mass in fibroblasts than in hPSCs, as reported (St John *et al*, 2005; Facucho-Oliveira *et al*, 2007). However, a similar mitochondrial mass per unit protein for hESCs, hIPSCs, and fibroblasts indicates that hPSCs and differentiated cells are equally committed to generating or maintaining mitochondria.

hPSC and differentiated cell mitochondria show similar O_2 consumption rates

hPSCs were examined to determine how much O_2 they consume. O_2 consumption rate (OCR) studies showed that intact hPSCs consume O_2 in room air at ~ 5–$8\,nmol\,O_2/min/ 5 \times 10^6$ cells (or ~ 1.0–$1.6\,fmol/min/cell$) (Figure 2A). By

contrast, fibroblasts consume O_2 at $\sim 13\text{--}15$ nmol O_2/min/ 5×10^6 cells (or $\sim 2.6\text{--}3.0$ fmol/min/cell) in room air, an ~ 2-fold higher rate than hPSCs. However, because there is ~ 1.5- to 2-fold more mitochondrial mass per fibroblast than hPSC, the OCR normalized to mitochondrial mass is $\sim$ equivalent between fibroblasts and hPSCs.

Electron transport chain (ETC) complexes I–IV transfer electrons from substrates to O_2 and the activity of each complex can vary between cell types. Substrate feeding into each ETC complex was performed with digitonin-treated HSF1 and HEK293 cells to determine relative complex activities. HEK293 cells were chosen because of a similar mitochondrial content (Figure 1B) and size (Supplementary Figure S1E) relative to hPSCs and for ease of substrate feeding compared with fibroblasts. Results show that ETC complex I–IV activities are similar between HSF1 and HEK293 cells (Supplementary Figure S2A) and, overall, the data indicate that hPSCs have a functional respiratory chain and OCR similar to fibroblasts when normalized to mitochondrial mass.

hPSCs are programmed for glycolysis

Different cell types in distinct microenvironments rely upon different bioenergetic processes for ATP production (Jezek *et al*, 2010). hPSCs and fibroblasts were therefore analysed for respiration and glycolysis in the same environment. To do this, OCR and the extracellular acidification rate (ECAR), which can approximate glycolysis from lactate production (Xie *et al*, 2009), were determined using a XF24 Extracellular Flux Analyser (Wu *et al*, 2007). The XF24 measures the rates of change in pmol O_2 and mpH simultaneously for cultured cells, providing a comparison for a defined cell population. For accurate analyses, hPSCs were plated with ROCK inhibitor (Watanabe *et al*, 2007) to form monolayers. Control or ROCK inhibitor-treated fibroblasts showed no statistical difference in the OCR/ECAR ratio (Supplementary Figure S2B). The number of cells seeded per well was adjusted for the linear range of measurements (Supplementary Figure S2C and D).

The OCR/ECAR ratios at two cell densities for hESCs and hIPSCs are $\sim 50\text{--}65\%$ lower than for fetal-derived NHDFs (Figure 2B) and ECAR values for hPSCs are ~ 1.5- to 2-fold higher than for fibroblasts (Figure 2C). Analysis of adult-origin fibroblasts (NHDFs) showed results that were statistically similar to those obtained with fetal-derived fibroblasts (Supplementary Figure S2E). These data suggest that hPSC bioenergetics favours glycolysis over OXPHOS, in contrast to fibroblasts. Addition of the competitive glycolysis inhibitor, 2-deoxyglucose (2-DG), causes hPSCs to G2 arrest (Figure 2D) and to minimally increase apoptosis (Supplementary Figure S2F) rather than shifting to respiration in room air, suggesting an immutable energetic preference. To determine a glycolytic transition with differentiation, HSF1 cells were exposed to RA and ECAR measured over time. Results showed a gradual and significant decrease in glycolysis with differentiation, with decreased ECAR (Figure 2E) and lactate in the culture media (Supplementary Figure S2G), indicating a progressive metabolic reprogramming during differentiation. Notably, hPSC OCRs and ECARs are mainly unaffected by 5–25 mM glucose (Supplementary Figure S2H) or by 0–17.5 mM insulin (Supplementary Figure S2I) incubations, indicating that the glucose supplied in these studies is not limiting. Furthermore,

glucose transporters *GLUT1* (widely expressed) and *GLUT4* (insulin-regulated) are expressed at $\sim$ equivalent high or barely detectable levels in hPSCs and fibroblasts, respectively (Supplementary Figure S2J and K), indicating an equivalent ability to bind and uptake glucose. Combined, the data strongly suggest that differences in OCRs and ECARs between hPSCs and differentiated cells are not from differences in glucose uptake but rather from unique intracellular metabolic programmes.

hPSCs are more sensitive to glycolysis inhibitors than are differentiated cells

OXPHOS was inhibited with oligomycin, a F_1F_0 ATP synthase inhibitor. Fibroblasts showed an $\sim 80\%$ reduction in O_2 consumption within 10 min (Figure 3A). By contrast, hPSCs showed an $\sim 50\%$ decrease in OCR, suggesting that hPSC are less dependent on OXPHOS than fibroblasts. Notably, there is a greater compensatory increase in ECAR for differentiated cells than for hPSCs with oligomycin exposure (Supplementary Figure S3A). Supplementary glucose (from 2.5 mM to 25 mM) maximized ECAR, with fibroblasts increasing $\sim 55\%$ in 20 min, whereas hPSC ECAR increased by a more modest $\sim 20\text{--}30\%$ (Figure 3B), indicating that hPSCs are closer to their maximal glycolytic capacity compared with fibroblasts. Following additions of 2-DG, which competes for uptake with glucose, hPSC glycolysis was repressed $\sim 65\%$ from the ECAR maximum within 34 min, whereas fibroblast glycolysis did not change for 6 min and then fell by only $\sim 45\%$ from the ECAR maximum after 34 min (Figure 3B), indicating that the hPSC glycolysis level is greater than in fibroblasts. Combined, the data indicate that hPSCs are less sensitive to OXPHOS inhibition, more sensitive to glycolysis disruption, and function closer to their maximum glycolytic capacity than do fibroblasts.

ATP in hPSCs is mainly produced by glycolysis

The steady-state ATP level is ~ 2-fold higher per cell in fibroblasts than in hPSCs, reflecting ATP production, consumption, and the size difference between these two cell types (Supplementary Figure S3B). OXPHOS inhibition with 0.1 μM oligomycin caused an $\sim 30\%$ ATP drop in fibroblasts, whereas the ATP drop in hPSCs was $< 5\%$ (Figure 3C), suggesting that hPSCs produce minimal ATP by OXPHOS. By contrast, sodium oxamate, a lactate dehydrogenase inhibitor that blocks ATP production by glycolysis, caused the ATP level in hPSCs to drop $> 60\%$, whereas fibroblasts showed $< 40\%$ ATP reduction (Figure 3D), indicating that hPSCs depend more on glycolysis for ATP production than do fibroblasts. ATP reductions with short-term inhibitor exposures are not due to a significant increase in cell death (Supplementary Figure S3C). Combined, the data indicate that the ATP level in hPSCs is sensitive to glycolysis inhibition.

hPSCs consume O_2 at maximal capacity

Although hPSC and fibroblast mitochondria consume O_2 at an $\sim$ equivalent rate, it is unclear what proportion of their maximal electron transport capacity is being utilized. FCCP is a mitochondrial uncoupler (protonophore) that dissipates the mitochondrial membrane potential ($\Delta\psi$) to stimulate maximal electron transport and O_2 consumption (Heytler, 1979). hPSCs failed to increase OCR, whereas fibroblasts showed an
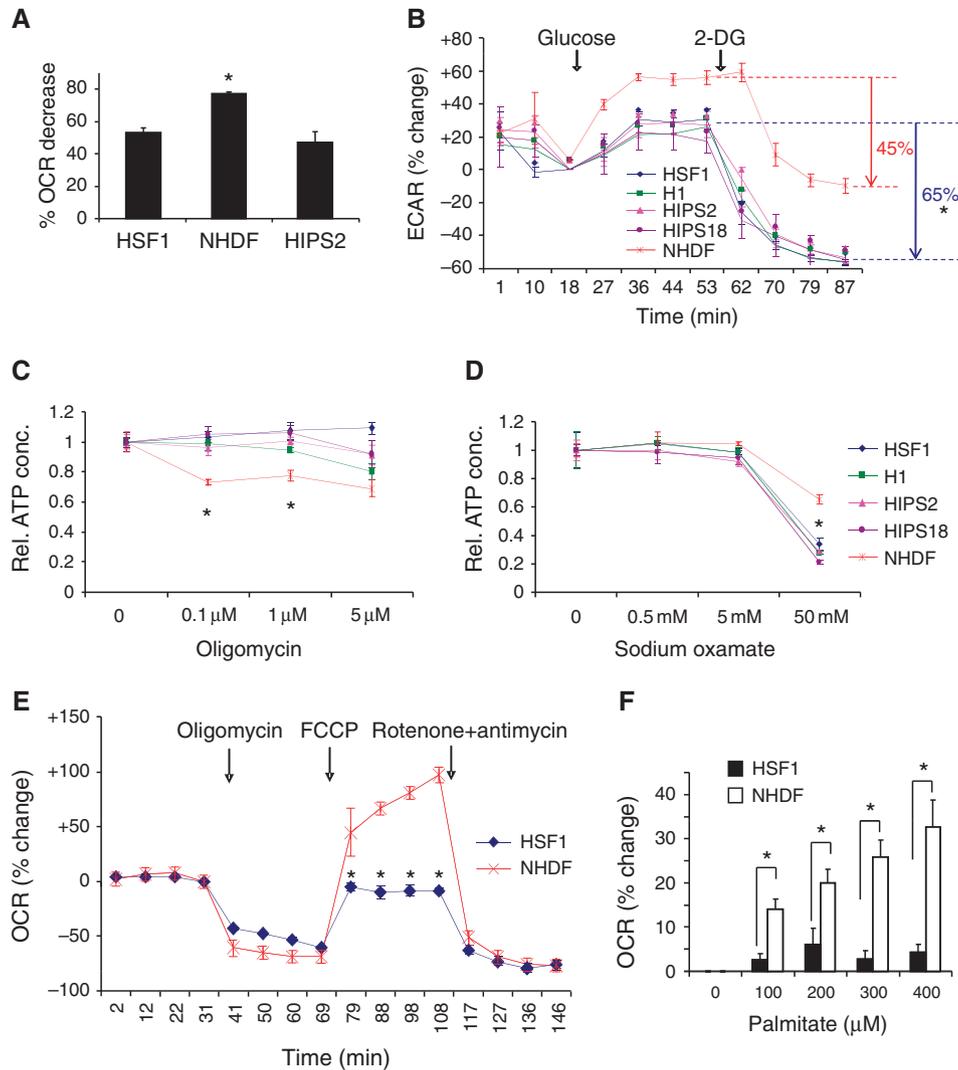
Figure 3 hPSCs require glycolysis for ATP production despite maximal O_2 consumption. (**A**) OCR change with 1 μM oligomycin for 10 min. Data are expressed as mean ± s.d. ($n = 3$), *$P < 0.05$. (**B**) Cells were cultured in assay medium with 2.5 mM glucose. ECAR change with glucose (25 mM final) and 2-DG (150 mM final) additions is shown. Arrows indicate percentage reduction from maximal ECAR ($n = 3$), *$P < 0.05$. (**C**) Change in cellular ATP with increasing doses of oligomycin at 45 min ($n = 3$), *$P < 0.05$. (**D**) Change in cellular ATP with increasing doses of sodium oxamate at 45 min ($n = 3$), *$P < 0.05$. (**E**) OCR changes in response to F_1F_0 ATP synthase inhibitor (1 μM oligomycin), uncoupler (0.3 μM FCCP), and ETC blockade (1 μM rotenone plus 1 μM antimycin) ($n = 3$), *$P < 0.05$. OCR due to non-mitochondrial sources is the distance between the post-rotenone + antimycin OCR (time points 127–146 min) and the abscissa. (**F**) OCR change in response to increasing doses of palmitate ($n = 3$), *$P < 0.05$.

∼90–100% increase in OCR at 0.1–0.4 μM FCCP exposures (Supplementary Figure S3D). To establish a baseline at which coupled respiration is inhibited, HSF1 cells and fibroblasts were exposed to 1 μM oligomycin to prevent proton movement through the F_1F_0 ATP synthase (Figure 3E). No significant changes in cell viability were detected during the course of oligomycin exposure (Supplementary Figure S3C). Addition of 0.3 μM FCCP re-establishes proton movement and results in maximal O_2 consumption. Then, incubation with rotenone and antimycin (complex I and III inhibitors, respectively) completely blocked mitochondrial respiration. The maximal mitochondrial respiration capacity is the difference between blocked and FCCP-induced OCR. Maximal hPSC respiration is equivalent to its pre-oligomycin respiration, which contrasts with the up to ∼100% increase in OCR measured for fibroblasts (Figure 3E). OCR does not increase further for hPSCs with increased sodium pyruvate supplemented media and FCCP exposure, excluding limited

substrate as a cause for an hPSC ceiling (Supplementary Figure S3E). Because oligomycin inhibits and FCCP stimulates OCR in coupled mitochondria, the smaller difference between FCCP-stimulated and oligomycin-inhibited OCR also suggests that hPSC mitochondria could be less coupled for ATP synthesis than fibroblast mitochondria (Supplementary Figure S3E). Finally, free fatty acid palmitate, an OXPHOS substrate, was added to cells incubated with L-carnitine, which transports fatty acids from the cytosol into the mitochondria. In contrast to fibroblasts that showed a dose-dependent OCR increase of ∼35%, HSF1 cells showed only a dose-independent ∼5% OCR increase (Figure 3F). The lack of a robust free fatty acid response in HSF1 cells could be from ETC saturation with glucose or internally produced fatty acids. Notably, the essential enzymes for fatty acid oxidation are equally expressed in HSF1 cells and fibroblasts by QPCR analysis. Combined, these data show that hPSCs consume O_2 at maximal capacity.
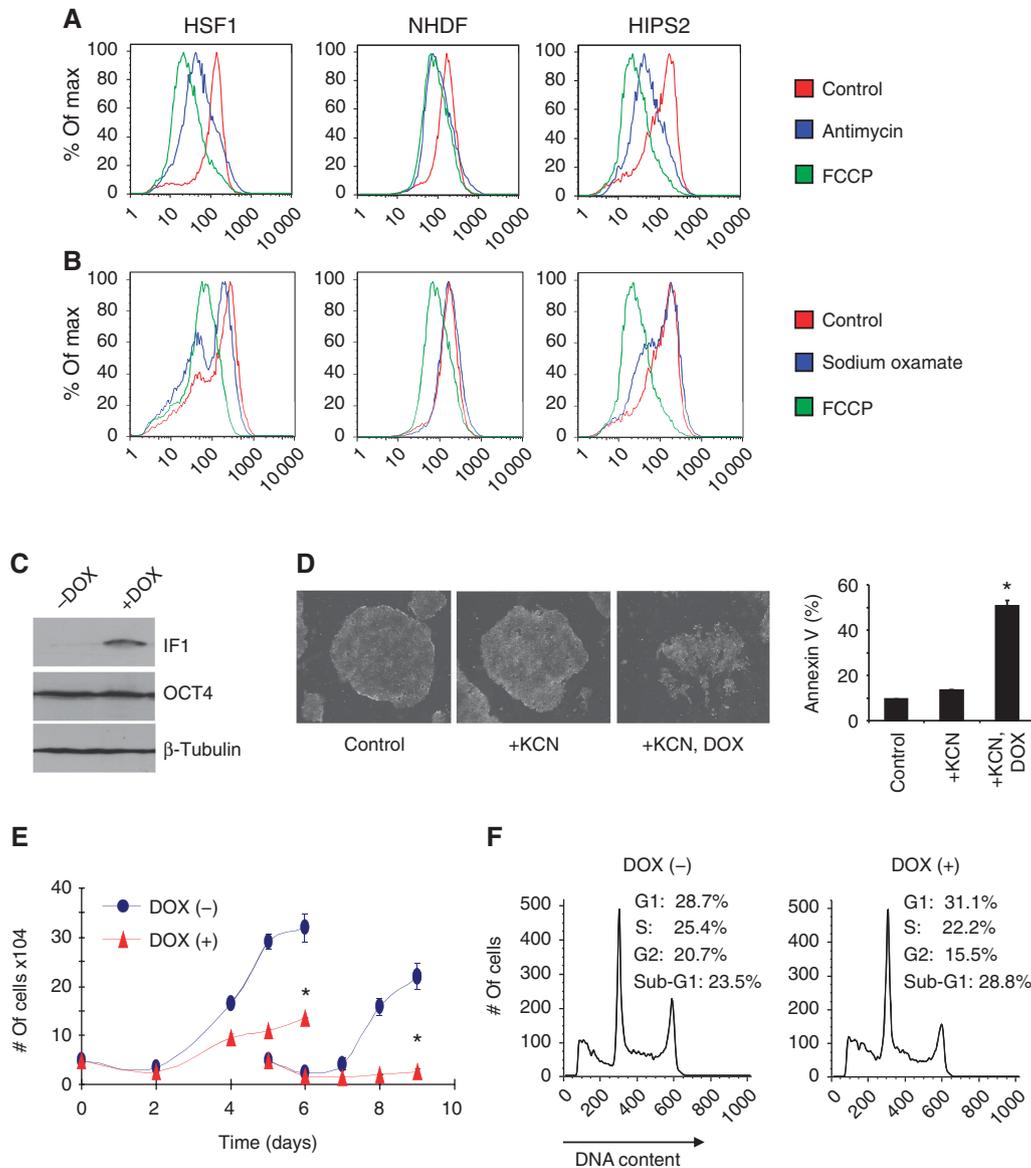
Figure 4 ATP hydrolysis maintains $\Delta\psi$, viability, and proliferation of hPSCs. (**A**) Dissipation of $\Delta\psi$ with antimycin (10 μM, 10 min) or FCCP (0.3 μM, 45 min) determined by $\Delta\psi$-sensitive TMRM dye staining and flow cytometry ($n = 2$). (**B**) Dissipation of $\Delta\psi$ with sodium oxamate (50 mM, 45 min) or FCCP analysed as described for (**A**). (**C**) Representative western blot of H1 hESCs transduced with a DOX-inducible IF1 lentiviral expression construct, with or without 2 μg/ml DOX for 3 days. (**D**) Representative colony morphology and percent Annexin V-positive cells for DOX-inducible IF1-containing H1 hESCs, with or without DOX and 1 mM KCN at 3 days. Data are expressed as mean ± s.d. ($n = 3$), *$P < 0.05$. (**E**) Cell counts of DOX-inducible IF1-containing H1 cells, with or without DOX. In all, 5×10^4 cells were plated after 3 days of DOX. Live cells were counted every other day. Cells were split at 4 days, re-plated at 5×10^4 cells/well, and counted until 9 days. Data are expressed as mean ± s.d. ($n = 3$), *$P < 0.05$. (**F**) Representative cell-cycle analysis of DOX-inducible IF1-containing H1 hESCs, with or without DOX at 3 days ($n = 3$).

Glycolytic ATP hydrolysis helps to maintain $\Delta\psi$ in hPSCs

A reduction in $\Delta\psi$ has been linked to mitochondrial dysfunction and possible mitophagy (Narendra *et al*, 2008). The presence of PARKIN protein expression in HSF1 cells that increases with RA-induced differentiation is consistent with the need to maintain $\Delta\psi$ in hPSCs (Supplementary Figure S4A), although this suggestion requires further investigation (Narendra *et al*, 2008, 2010). In differentiated cells, $\Delta\psi$ is maintained by a proton gradient formed during the passage of electrons through the ETC. Alternatively, $\Delta\psi$ is maintained by hydrolysis of glycolytic ATP in the F_1F_0 ATP synthase when ETC function is reduced (Nicholls and Lindberg, 1972; Hatefi, 1985). For mouse ESCs, the relative level of $\Delta\psi$ has a role in

regulating differentiation (Schieke *et al*, 2008). Therefore, the mechanism(s) for hPSC $\Delta\psi$ maintenance was examined. Immunofluorescence microscopy showed an intact $\Delta\psi$ for all HSF1 mitochondria imaged that was dissipated with 100 μM FCCP (Supplementary Figure S4B). To determine what portion of $\Delta\psi$ is provided by electron transport versus hydrolysis of glycolytic ATP, antimycin was used to dissipate the ETC-generated component of $\Delta\psi$ and sodium oxamate was used to dissipate the glycolysis-generated component of $\Delta\psi$, followed by quantification using $\Delta\psi$-sensitive TMRM staining and flow cytometry. Antimycin and FCCP equivalently and robustly dissipate $\Delta\psi$ in fibroblasts, whereas antimycin only partially dissipates $\Delta\psi$ in hPSCs (Figure 4A;
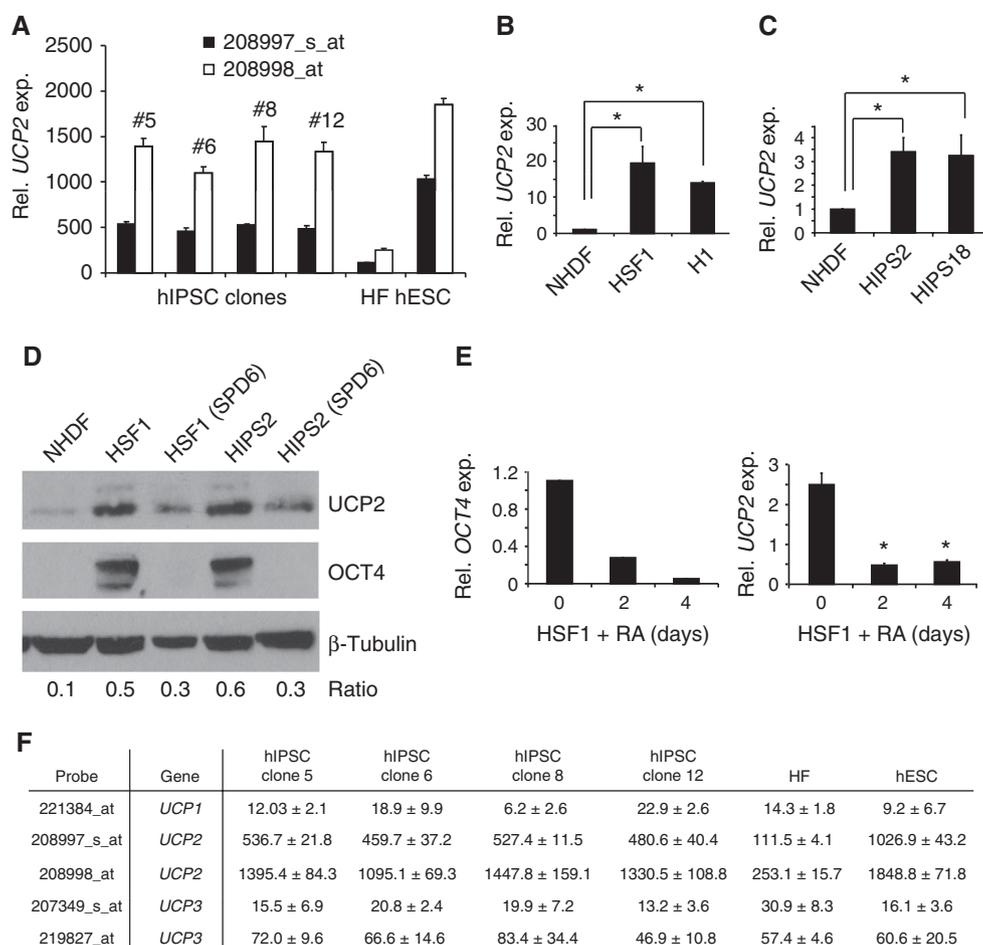
Figure 5 UCP2 is highly expressed in hPSCs and is repressed during differentiation. (**A**) *In-silico* analyses of *UCP2* expression from expression profiling studies (Maherali *et al*, 2008). Two probes detecting *UCP2* RNA are shown. HF, human fibroblasts. (**B, C**) *UCP2* expression by QPCR ($n=3$), *$P<0.05$. (**D**) Western blots under native conditions and conditions that promote hPSC differentiation. SPD6: media change-induced differentiation by replacing 20% KSR with 20% FBS for 6 days. (**E**) *OCT4* and *UCP2* expression by QPCR with 10 μM RA-induced differentiation for 4 days ($n=3$), *$P<0.05$. (**F**) *In-silico* analysis of *UCP1*, *UCP2*, and *UCP3* expression from expression profiling studies in the same lines as in (**A**) (Maherali *et al*, 2008).

Supplementary Figure S4C, with JC-1 staining). Sodium oxamate partially dissipates Δψ in hPSCs but had no effect on Δψ in fibroblasts (Figure 4B). Combined, the data indicate that Δψ in fibroblasts is maintained by the ETC, whereas Δψ in hPSCs is partially maintained by glycolysis.

In differentiated cells with an impaired ETC, ATP hydrolysis maintains Δψ, proliferation, and viability (Buchet and Godinot, 1998). Conversion of F_1F_0 ATP synthase to hydrolase activity is blocked by inhibitory factor-1 (IF1) (Campanella *et al*, 2008). Notably, the ratio of IF1 to the F_1F_0 ATP synthase β-subunit protein, which is the target of IF1 (Ichikawa *et al*, 2005), is significantly lower in hPSCs than in differentiated cells, which is suggestive of a potential ATP hydrolase function for the F_1F_0 ATP synthase in hPSCs (Supplementary Figure S4D). To investigate this possibility, a doxycycline-inducible IF1 lentiviral expression construct was transduced into H1 hESCs (Figure 4C), followed by ETC impairment using KCN, a complex IV inhibitor. hPSCs with ectopic IF1 expression showed abundant cell death in KCN (Figure 4D). Notably, ectopic IF1-expressing H1 cells with intact ETC activity in room air also showed a significant growth defect in extended culture (Figure 4E) due to increases in G_0/G_1 phase of the cell cycle and apoptosis

(Figure 4D and F). Combined, the data suggest that the ATP hydrolase activity of the F_1F_0 ATP synthase is essential for maintaining the Δψ, proliferation, and viability of hPSCs.

UCP2 is expressed in hPSCs and repressed during differentiation

To identify a mechanism(s) controlling the unique mitochondrial metabolism of hPSCs, we re-analysed three expression profiling studies to search for metabolism-regulating genes that were differentially expressed between hPSCs and differentiated cells. Two studies compared gene expression between hPSCs and fibroblasts (Lowry *et al*, 2008; Maherali *et al*, 2008) and a third study evaluated gene expression with hESC differentiation to embryoid bodies (EBs) and cardiomyocytes (Cao *et al*, 2008). Notably, *UCP2* expression was 5- to 10-fold higher in hPSCs than in human fibroblasts (Figure 5A; Supplementary Figure S5A) and ~30–40% lower in EBs and cardiomyocytes than in hESCs (Supplementary Figure S5B). Validating these *in-silico* data, *UCP2* gene and protein expression was significantly higher in hPSCs than in differentiated cells (Figure 5B–D; Supplementary Figure S5C). HSF1 and HIPS2 cells were stimulated to differentiate by medium replacement (20% KSR→20% FBS) (Figure 5D)

or HSF1 cells were induced to differentiate by replacing bFGF with 10 μM RA (Figure 5E). *UCP2* was repressed in both settings. In contrast to *UCP2*, *UCP1* and *UCP3* expression was very low or absent in hPSCs (Figure 5F). UCP2 and UCP3 typically account for 0.01–0.1% of mitochondrial inner membrane proteins, whereas UCP1, whose expression is confined to brown adipose tissue cells, accounts for up to 10% of the inner membrane protein mass (Brand and Esteves, 2005). Comparatively abundant *UCP2* expression suggests potential functional significance in hPSCs.

UCP2 is a regulator of hPSC energy metabolism
UCP2 stimulates aerobic glycolysis in leukaemia cells (Samudio *et al*, 2008, 2009; Bouillaud, 2009) and one hypothesized, but experimentally untested mechanism for UCP2 activity based on UCP1 studies is to shunt pyruvate out of mitochondria, thereby reducing glucose oxidation in mitochondria and increasing glycolytic flux (Bouillaud, 2009; Samudio *et al*, 2009). UCP2 expression in hPSCs suggests that it could regulate hPSC glucose metabolism. To test this hypothesis, *shUCP2* HSF1 cells were generated. *shUCP2* cells retained OCT4 (Figure 6A) and SSEA4 (Supplementary Figure S6A) pluripotency markers with an ~33% decrease in ECAR (Figure 6B) and an ~40% decrease in cellular ATP (Figure 6C), indicating reduced metabolic activity compared with control cells without affecting the expression of OCT4. A similar decrease in ECAR occurred with a second *shUCP2* construct in HSF1 cells (Supplementary Figure S6B). *shUCP2* also reduced ECAR in highly proliferative HEK293 cells that express UCP2 at a level similar to hPSCs, suggesting a conserved metabolic regulatory mechanism for UCP2-expressing cells (Supplementary Figure S6C and D).

UCP2 has been postulated to block glucose-derived pyruvate oxidation in mitochondria (Jezek and Garlid, 1990; Jezek and Borecky, 1998; Bouillaud, 2009). Therefore, UCP2 repression could maintain or enhance mitochondrial oxidation of glucose in differentiated cells. To test this idea, *UCP2* was ectopically expressed during early hPSC differentiation (Figure 6D and E). HSF1 cells exposed to RA for 6 days showed a >2-fold increase in the OCR/ECAR ratio, indicating a transition from glycolysis to mitochondrial glucose oxidation, whereas ectopic *UCP2* expression blocked this transition as shown by an almost unchanged OCR/ECAR ratio before and after differentiation (Figure 6F). Interestingly, *UCP2* expression repressed OCR in differentiated cells, consistent with UCP2 blocking mitochondrial glucose oxidation (Figure 6G). In order to further test this hypothesized mechanism for UCP2 regulation of metabolism, stable isotope tracing studies were performed to determine whether UCP2 directly prevents pyruvate from entering into mitochondrial oxidation. Cells were incubated in media supplemented with [U^{13}C$_6$]-labelled glucose, during which the expression of UCP2 and pluripotent transcription factors were unaltered (Supplementary Figure S6E). Labelled glucose is converted to pyruvate, which then enters mitochondria and is further oxidized into different mass isotopomers of TCA cycle intermediates, such as α-ketoglutarate (Lee *et al*, 2010). Since α-ketoglutarate is in equilibrium with glutamate, the isotopomers of glutamate were used to measure the amount of labelled glucose contributing to mitochondrial oxidation (Boren *et al*, 2003). Ectopic *UCP2* expression had no significant effect

on glucose oxidation in undifferentiated hPSCs (Figure 6H), possibly because of already high UCP2 expression (Figure 5). By contrast, a significant ~13% decrease in ^{13}C incorporation into glutamate (Σmn) was detected in RA-differentiated hPSCs (Figure 6H), indicating UCP2 impairs glucose oxidation. Notably, RA-induced differentiation also caused an ~13% decrease in glucose oxidation, likely from reduced proliferation and resultant lowered overall metabolism with differentiation (see Supplementary Figure S7A). Ectopic UCP2 expression also increased the amount of ribose generated from glucose by ~30% in undifferentiated hPSCs and by ~12% with hPSC differentiation (Figure 6I), strongly supporting a role for UCP2 expression in shunting pyruvate away from oxidation in mitochondria and towards the pentose phosphate pathway via an increased glycolytic flux. Combined, the data show that UCP2 repression during differentiation is required to transition from glycolysis to glucose oxidation in mitochondria.

To determine whether UCP2-mediated uncoupling contributes to this metabolic transition, the effect of oligomycin and FCCP was examined in *UCP2* knockdown and ectopic-expression HSF1 cells. Neither manipulation altered responses to oligomycin nor FCCP compared with control hPSCs (Supplementary Figure S6F). Ectopic *UCP2* expression also did not increase OCR (Figure 6G) as uncouplers do. The data suggest that UCP2 does not function like UCP1 with its established uncoupling activity, but rather UCP2 helps to regulate hPSC bioenergetics by controlling substrate access to oxidation in mitochondria.

UCP2 impacts ROS and differentiation potential of hPSCs
Reactive oxygen species (ROS) are respiration by-products that cause oxidative damage to proteins, lipids, and DNA. ROS also increases with hPSC differentiation (Cho *et al*, 2006; Saretzki *et al*, 2008). In immune cells, UCP2 attenuates ROS accumulation (Echtay *et al*, 2001). To evaluate UCP2 in hPSC ROS regulation, ROS was measured in control and *shUCP2* HSF1 cells. The data show that ROS was substantially increased with *shUCP2* (Figure 7A) and resulted in elevated hPSC apoptosis (Figure 7B). Ectopic *UCP2*-expressing HSF1 cells showed decreased ROS compared with control cells (Figure 7C, panels i, iv, and vii). By contrast, HSF1 cells with or without ectopic *UCP2* expression induced to differentiate for 2 days by media-replacement (20% KSR→20% FBS, or spontaneous differentiation day 2 (SPD2)) showed increased ROS accumulation (Figure 7C, panels iii and vi). However, ectopic *UCP2*-expressing HSF1-differentiated cells show less ROS than differentiated control cells (Figure 7C, panel viii), indicating that *UCP2* repression with differentiation contributes to ROS accumulation.

The data thus far show that UCP2 helps to regulate metabolic reprogramming during hPSC differentiation. Whether this regulation contributes to hPSC differentiation is unknown. To address this critical question, EB formation, as a measure of differentiation, was determined with control and ectopic *UCP2*-expressing HSF1 cells. Strikingly, ectopic *UCP2* expression caused significant defects in EB quantity and quality (Figure 7D). Ectopic *UCP2* expression did not alter the expression of developmental genes representing the three-germ layers of the definitive embryo or the trophoblast lineage in hPSCs (Figure 7E) as they are all lowly expressed
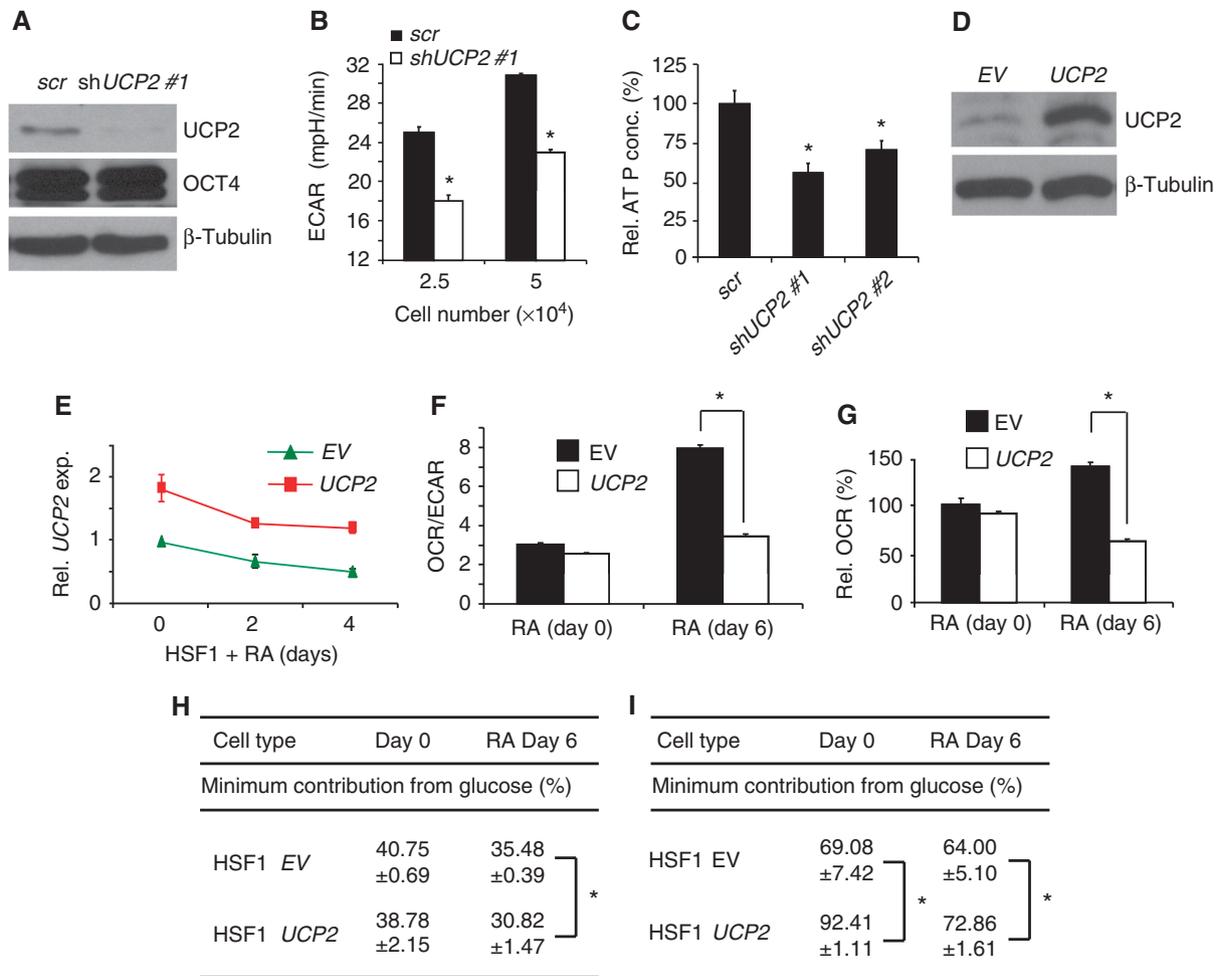
Figure 6 UCP2 regulates energy metabolism in hPSCs and during differentiation. (**A**) Western blots in HSF1 cells transduced with *shUCP2 #1* and a scramble (*scr*) control. (**B**) ECAR for *shUCP2 #1* and *scr* HSF1 cells ($n=3$), *$P<0.05$. (**C**) ATP normalized for HSF1 cell number with *shUCP2* knockdown ($n=3$), *$P<0.05$. (**D**) UCP2 immunoblot in HSF1 cells transduced with empty vector and *UCP2*-expressing lentiviruses. (**E**) *UCP2* expression by QPCR in *EV* and *UCP2* transduced HSF1 cells with 10 μM RA-induced differentiation for up to 4 days ($n=3$). (**F, G**) OCR/ECAR and OCR for *EV* or *UCP2* transduced HSF1 cells exposed to 10 μM RA for up to 6 days ($n=3-7$), *$P<0.005$. (**H**) Stable isotope tracing analysis. hPSCs were grown in StemPro SFM medium (17.5 mM glucose) supplemented with 7.5 mM [$U^{13}C_6$]-labelled glucose for 48 h. $\sum mn$ (average ^{13}C/molecule) was calculated from the mass isotopomer distribution in glutamate. Minimum contribution from glucose was calculated through dividing the observed $\sum mn_{glutamate}$ by the theoretical $\sum mn_{glutamate}$ ($7.5/25 \times 4$), when all glucose carbons become $\sum mn$ carbons in the C2–C5 fragment of glutamate. Data are expressed as mean ± s.d. ($n=3$). (**I**) Stable isotope tracing analysis with cells grown as in (**H**), $\sum mn$ was calculated from the mass isotopomer distribution in ribose. The minimum contribution from glucose was calculated through dividing the observed $\sum mn_{ribose}$ by the theoretical $\sum mn_{ribose}$ ($7.5/25 \times 5$). Data are expressed as mean ± s.d. ($n=3$), *$P<0.05$.

before differentiation. By contrast, *UCP2* significantly impaired the induction of these developmental genes in hPSCs induced to differentiate with RA (Figure 7E) without affecting cell proliferation or viability (Supplementary Figure S7A). Notably, addition of ROS scavengers such as *N*-acetyl-cysteine or glutathione did not change the repression of differentiation from ectopic *UCP2* expression (Supplementary Figure S7B and C), strongly suggesting that ROS is not the main factor in UCP2 regulation of hPSC differentiation. Instead, the data show that UCP2 is a metabolic regulator of hPSC differentiation and its repression facilitates a metabolic transition favouring oxidative metabolism, which is required for the proper early differentiation of hPSCs.

Discussion

Little is known and much is assumed about hPSC energy production and utilization. Here, we show that hPSCs are

'hardwired' for metabolic activity that is heavily skewed towards glycolysis. ATP from glycolysis is used to meet energy and biosynthetic demands and to maintain Δψ in support of cell proliferation and viability. Despite their under-developed appearance, hPSC mitochondria contain functional ETC complexes and consume O_2 maximally, although they rely mainly on glycolytic ATP compared with differentiated cells, such as fibroblasts. There is a shift from glycolysis to OXPHOS that becomes more pronounced as hPSCs progressively differentiate. UCP2 expression is repressed with hPSC differentiation, and this repression is necessary for a proper shift from glycolysis to mitochondrial glucose oxidation. Ectopic *UCP2* expression during early differentiation impairs this metabolic transition, retards ROS accumulation, and inhibits EB formation and differentiated gene induction. These unique metabolic features are conserved in multiple hESC and hIPSC lines, suggesting that hPSC energy metabolism is an underappreciated pre-set programme and a core
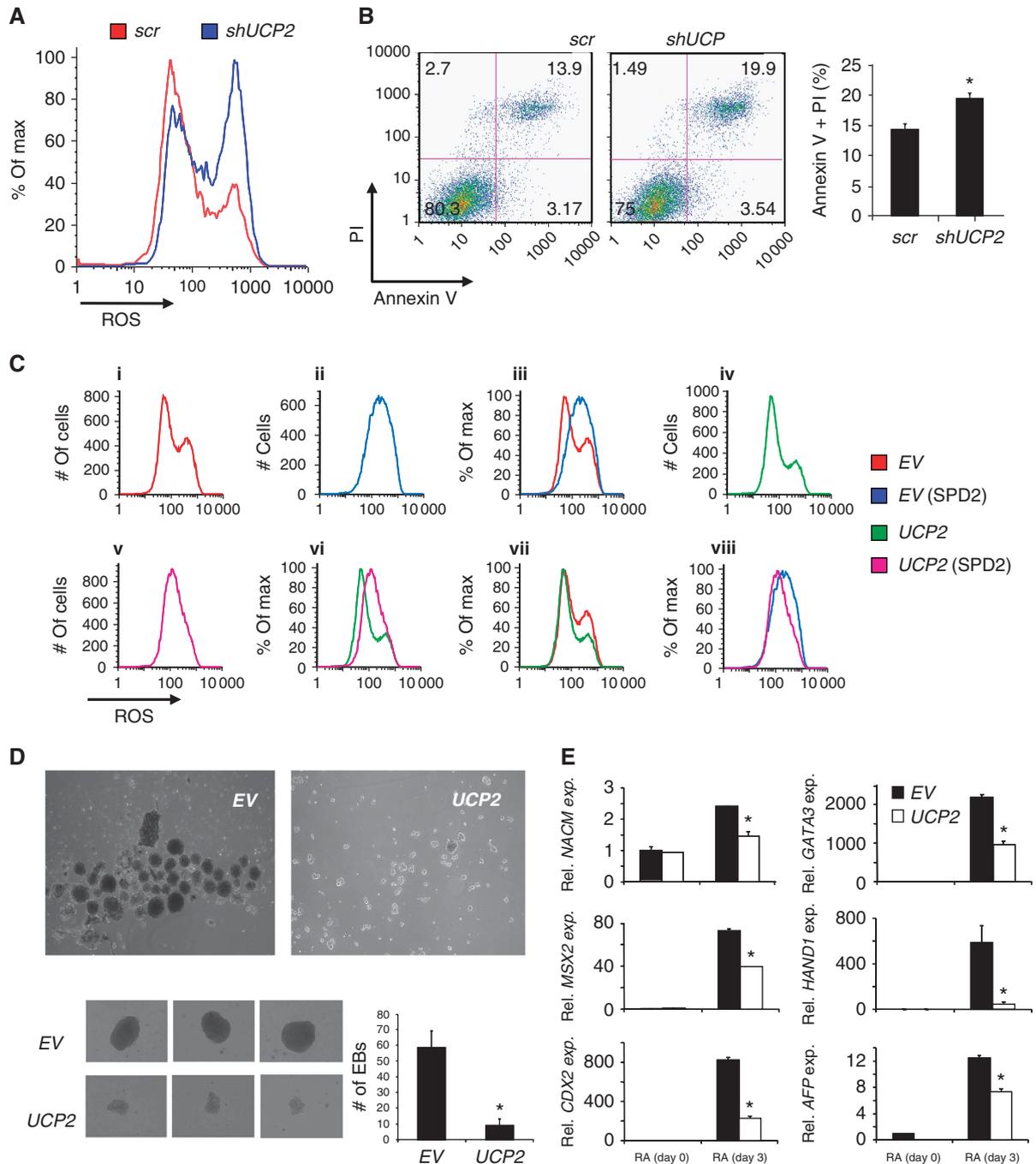
Figure 7 UCP2 regulates ROS, hPSC viability, and differentiation. (**A**) Representative ROS determination in transduced HSF1 cells by 2-dihydroethidium staining and flow cytometry ($n = 3$). (**B**) Apoptosis staining and flow cytometry. Data are plotted in the right panel. Data are expressed as mean ± s.d. ($n = 3$), *$P < 0.05$. (**C**) ROS determination in transduced HSF1 cells with or without differentiation induction by media replacement for 2 days (SPD2). Panel (iii) is an overlay of (i, ii); panel (vi) is an overlay of (iv, v); panel (vii) is an overlay of (i, iv); and panel (viii) is an overlay of (ii, v). (**D**) EB formation assay with transduced HSF1 cells. Data are expressed as mean ± s.d. ($n = 3$), *$P < 0.05$. (**E**) mRNA expression of developmental genes in transduced HSF1 cells. Data are expressed as mean ± s.d. ($n = 3$), *$P < 0.05$.

component of 'stemness', similar to the epigenetic and genetic programmes that maintain hPSC self-renewal (Boyer *et al*, 2005; Meshorer and Misteli, 2006).

Support for an hPSC metabolic programme comes from several lines of evidence. First, glycolysis is the main ATP production mechanism, regardless of O_2 availability, with hPSCs grown in ambient O_2 utilizing glycolysis in preference to OXPHOS outside of the hypoxic blastocyst inner cell mass (Fischer and Bavister, 1993). Second, hPSC mitochondria hydrolyze glycolytic ATP to partially maintain $\Delta\psi$, which is

required for cell proliferation and survival. By contrast, differentiated cell mitochondria do not hydrolyze appreciable glycolytic ATP unless their ETC becomes compromised (Buchet and Godinot, 1998; Campanella *et al*, 2008). hESCs in room air with intact ETC functions show reduced proliferation and viability with IF1-induced F_1F_0 ATP hydrolase inhibition, rather than adapting to OXPHOS to maintain $\Delta\psi$. Third, hPSCs proliferate rapidly compared with most differentiated cell types (Supplementary Figure S7D) (Becker *et al*, 2006), and they may require a high glycolytic flux to support

anabolic metabolism. Glycolysis provides intermediate metabolites such as ribose and NADPH from the pentose phosphate pathway for nucleotide and lipid biosynthesis (DeBerardinis *et al*, 2008). In addition to a gradual decrease in glycolysis with differentiation (Figure 2E), QPCR showed that most key enzymes in the pentose phosphate pathway and lipid biosynthesis pathways are repressed during media-replacement or RA-induced differentiation (Supplementary Figure S7E and F). Finally, hESCs typically die or differentiate with oxidative stress (Saretzki *et al*, 2008) or the DNA damage that results from oxidative stress (Lin *et al*, 2005). Mouse ESCs and hESCs also show elevated ROS with differentiation, and ROS is a known DNA mutagen (Sauer *et al*, 2000; Cho *et al*, 2006). The impact of UCP2 on hPSC metabolism provides a potential mechanism by which hPSCs reduce ROS to maintain genomic integrity and cell viability.

Distinct bioenergetic metabolism in hPSCs and during early differentiation or reprogramming suggests a coordinated molecular switching mechanism of unknown origin. Here, we show that UCP2 is a molecular regulator of hPSC energy metabolism, although it is most likely one of the several thus far unidentified regulators of hPSC metabolism. *UCP2* knockdown shifts hPSC bioenergetics away from glycolysis, whereas ectopic *UCP2* expression blocks glucose oxidation. In Supplementary Figure S7G, we provide a simple model for our study results and the mechanism for UPC2 regulation of hPSC metabolism based upon the study results. In hPSCs, UCP2 shunts substrates such as pyruvate from glucose oxidation, favouring glycolysis and nucleotide biosynthesis through the pentose phosphate shunt pathway. Glycolysis provides ATP to partially maintain $\Delta\psi$ in hPSC mitochondria. In early hPSC differentiation, overall cell metabolism drops with reduced proliferation, glycolysis, and glucose oxidation in parallel with UCP2 repression. Physiologic *UCP2* repression sustains glucose oxidation, ATP production, and provides TCA cycle intermediates which could be important co-factors for hPSC differentiation, such as α-ketoglutarate, which is required for the activity of epigenetic enzymes that regulate gene expression (Figueroa *et al*, 2010; Xu *et al*, 2011). Disruption of *UCP2* repression interrupts this metabolic transition and blocks early hPSC differentiation. Lowered *UCP2* expression facilitates ROS accumulation, which could stimulate hPSC differentiation to certain lineages, such as cardiomyocytes. Since hIPSCs show a mitochondrial network structure, metabolic profile, and *UCP2* expression pattern similar to hESCs, the hPSC metabolism programme appears reversible with de-differentiation.

These results may have significant implications for utilizing hPSCs in emerging cell-based therapies in the clinic. When hPSCs are differentiated for tissue transplantation, residual undifferentiated cells, even if rare, could retain metabolic characteristics seen in human cancers, such as a high glycolytic flux, perhaps making them more prone to tumour formation. The characterization of mitochondria-related energy metabolism before and after hPSC differentiation, and the discovery of one molecular mechanism regulating a metabolic transition to oxidation during differentiation, will potentially aid in identifying hPSCs with reduced tumourigenic potential or the discovery of drugs targeting metabolic pathways that increase the safety of hPSC-based therapies in the future.

Materials and methods

Cell lines
hESCs and hIPSCs (Lowry *et al*, 2008) were grown on feeder-free Matrigel (BD Biosciences) in StemPro SFM medium (Invitrogen) for all experiments, as described (Khvorostov *et al*, 2008; Zhang *et al*, 2008a, b). Fibroblast and HEK293 cells were cultured in DMEM (Cellgro) with 10% FBS and supplements.

Fluorescence microscopy
Cells were fixed in 3.7% formaldehyde for 10 min, blocked in 0.2% BSA for 5 min, and incubated with OCT4 Ab (1:200; Cell Signaling) in 0.1% Triton-X100 and 1 × PBS, pH 7.4 overnight at 4°C, followed by staining with FITC-conjugated rabbit anti-IgG Ab (1:500; Jackson ImmunoResearch) for 1 h. For mitochondrial staining, 100 nM of either Δψ-dependent MitoTracker Red CMXRos or independent MitoTracker Green FM was added to the culture medium for 10 min at 37°C. A LSM 5 Pa laser scanning microscope (Zeiss) was used to visualize mitochondrial morphology.

Transmission electron microscopy
hPSCs were processed for TEM as described previously (Sun *et al*, 2007). Briefly, cells were fixed in a solution containing 3.0% formaldehyde, 1.5% glutaraldehyde in 100 mM cacodylate containing 2.5% sucrose, pH 7.4 and subsequently osmicated in Palade's OsO$_4$ (1 h at 4°C). The pellet was washed three times in 100 mM cacodylate, pH 7.4, treated with 1% tannic acid for 30 min at RT, washed three times in double-distilled water, and incubated overnight in Kellenberger's uranyl acetate. The pellet was then dehydrated through a graded series of ethanol and embedded in EMBED-812. Sections were cut on a Leica Ultracut UCT ultramicrotome, collected onto 400-mesh thin-bar nickel grids, post-stained with uranyl acetate and lead citrate, and observed in a Tecnai 12 at 100 kV. Images were collected with an Olympus SIS Megaview III CCD. The figures in Supplementary Figure S1B were assembled in Adobe Photoshop with only linear adjustments in brightness and contrast.

Citrate synthase assay
Whole-cell protein (8 µg/sample) was mixed with acetyl-CoA, 5,5′-dithiobis-2-nitrobenzoic acid (DTNB), and oxaloacetic acid in a 96-well plate and 412 nm absorption was recorded using a Citrate Synthase Assay kit (Sigma).

Immunoblotting
Cells were lysed in lysis buffer (50 mM Tris–HCl, pH 7.4, 150 mM NaCl, 1 mM EDTA, and 1% Triton-X100) containing 1 × protease inhibitor cocktail (Sigma). Protein (50 µg/lane) was resolved by 8–15% SDS–PAGE, transferred to nitrocellulose membranes, and incubated for 1 h with 5% milk TBS-T and overnight with primary Abs in 5% BSA. Abs included OCT4, PARKIN (Santa Cruz), TOM40, TIM23, IF1, β-TUBULIN (Abcam), and UCP2 (BioLegend). ECL Plus (GE Healthcare) was used for chemiluminescent detection.

O$_2$ consumption
A Clark-type O$_2$ electrode was used in a magnetically stirred, thermostatically controlled 0.3 ml chamber at 25°C (Oxytherm; Hansatech). Cells (5×10^6) in 300 µl buffer (0.137 M NaCl, 5 mM KCl, 0.7 mM NaH$_2$PO$_4$, 25 mM Tris–HCl, pH 7.4) were assessed for O$_2$ consumption. For determination of individual ETC complex activities, 0.03% digitonin was used to permeabilize cells. Complex activities were measured by feeding complex-specific substrates while inhibiting the prior complexes in the chain. OCR for complexes I–IV was measured by adding 8 mM pyruvate + 2.5 mM malate; OCR for complexes II–IV was measured by first inhibiting complex I with 3.3 µM rotenone followed by the addition of 10 mM succinate; OCR for complexes III–IV was measured by first inhibiting complex II with 10 mM malonate followed by the addition of 20 mM glycerophosphate; and OCR for complex IV was measured by first inhibiting complex III with 33 mM antimycin followed by the addition of 10 mM ascorbate plus 0.2 mM TMPD (tetramethyl-*p*-phenylenediamine).

Cell diameters
Measurements were made using the Countess® Automated Cell Counter (Invitrogen) according to the manufacturer's instructions.

XF24 extracellular flux analyser

hPSCs were seeded onto an XF24 Cell Culture Microplate (Seahorse Bioscience) at $2-7.5 \times 10^4$ cells/well with the ROCK inhibitor dihydrochloride (Sigma) (Watanabe *et al*, 2007) and incubated at 37°C overnight. Cell metabolic rates were measured using an XF24 Extracellular Flux Analyser (Seahorse Bioscience) in unbuffered DMEM assay medium supplemented with 1 mM pyruvate and 25 mM glucose after 45 to 60 min equilibration. For studies with palmitate addition, KHB assay medium (Seahorse Bioscience) supplemented with 500 μM L-carnitine was used. OCR and ECAR were normalized to protein concentration using the Protein Assay reagent (Bio-Rad) in all experiments.

Lactate quantification

Culture media (50 μl) was harvested per sample and lactate content was measured using a Lactate Assay kit (Biovision) according to the manufacturer's instructions.

ATP quantification

Cells (10^4/well) were incubated with oligomycin or sodium oxamate (Sigma) for 45 min at 37°C. The CellTiter-Glo Luminescent Cell Viability Assay kit (Promega) was used to assay for ATP. Luminescence intensity from each well was measured using a GloMax 96 Luminometer (Promega).

Mitochondrial membrane potential determination

$\Delta\psi$ was determined using a MitoPT TMRM Assay kit (Immuno-Chemistry Technologies) or BD MitoScreen kit (BD Biosciences Pharmingen) according to the manufacturers' instructions.

Lentiviral hPSC infection

The cDNA for *ATPIF1* (Gene ID 93974), encoding *IF1*, was cloned into the lentiviral vector pLTET1 (Vieyra and Goodell, 2007), which contains a tetracycline controlled promoter and dsRed expression cassette. Two UCP2 (TRCN0000060143 and TRCN0000060144) or scramble shRNAs in the lentiviral vector of pLKO were bought from Sigma. The cDNA for *UCP2* (Gene ID 7351) was cloned into a modified lentiviral vector *pCCL* with CMV promoter replaced by EF1α promoter. Lentivirus was made by transfecting 2×10^6 HEK293T cells with 10 μg lentiviral vector, 6.5 μg *pCMV-ΔR8.2* packaging vector, and 3.5 μg *pCMV-VSV-G* envelope vector using Fugene (Roche). Two days later, medium was collected, filtered, and virus concentrated using the Lenti-X concentrator (Clontech). Concentrated virus was added to HSF1 hESCs or H1 hESCs stably expressing the tetracycline transactivator, *rtTA2SM2* (Vieyra and Goodell, 2007), followed by mixing for 2 h at 37°C in the presence of 8 μg/μl polybrene, plating onto Matrigel plates in StemPro SFM medium.

Measurement of ROS

HSF1 cells (10^6) were trypsinized, collected, and washed by PBS. In all, 5 μM 2-dihydroethidium (Sigma) was added to cells followed by incubation at 37°C for 10 min. Stained cells were washed by PBS and applied to a BD FACSCalibur flow cytometer.

Reverse transcription and real-time PCR (QPCR)

Total RNA was extracted from hESCs, hIPSCs, fibroblasts, and HEK293 cells using Trizol reagent (Invitrogen). cDNA was synthesized using Superscript III first-strand cDNA synthesis kit (Invitrogen). Real-time PCR was performed using SYBR green real-time PCR kit (Diagenode) with denaturation 94°C; 15 s, annealing 60°C; 30 s, extension 72°C; 45 s for 40 cycles. Primer sequences are available upon request.

Cell-cycle analysis

Cells were stained in a hypotonic buffer containing 0.1 g/l propidium iodide, 1 g/l sodium citrate, 0.3% Triton-X100, and 0.02 g/l ribonuclease A for 5 min, and analysed on a BD FACSCalibur flow cytometer.

Embryoid body formation

EB formation was assessed using AggreWell400 plates (Stemcell Technologies) according to the manufacturer's instructions. In brief, 10^6 cells were plated and the next day EBs were harvested and further cultured in IMDM medium supplemented with 20% FBS for 10 days. An inverted light microscope was used to assess and count EB colonies.

Stable isotope tracing

Cells were cultured in StemPro SFM medium (17.5 mM unlabelled glucose) supplemented with 7.5 mM [U^{13}C$_6$]-glucose (Cambridge Isotope Laboratories) for 48 h. Three independent replicates of 2×10^6 cells for each line were collected, and the cell pellets were suspended in 0.5 ml of water and lysed by sonication. Cell debris was separated by centrifugation and proteins precipitated by treating the clear supernatant with 1 ml of cold acetone. The final supernatant was air-dried and the free glutamic acid was converted to its trifluoroacetamide butyl ester for GC/MS analysis (Lee *et al*, 1996). Glutamate mass isotopomers were determined from the m/z 198 cluster representing the C2–C5 fragment of glutamate. $\sum mn$, which is given by $m0 + m1 + 2 \times m2 + 3 \times m3 + \dots$, is the average ^{13}C per C2–C5 of the glutamate molecule and the equivalent of specific activity in radioisotope studies. The observed $\sum mn$ divided by the theoretical $\sum mn$ (calculated from $\sum mn$ of glucose adjusted for the difference in the number of carbons per molecule) provides an estimate of the contribution of glucose to the TCA cycle. For ribose, RNA was extracted with TriReagent (Sigma, Cat#T9424). Ribose was isolated after RNA acid hydrolysis with 2 N HCl and derivatization into its aldonitrile acetate derivative for GC/MS analysis (Lee *et al*, 1998). The observed $\sum mn$ divided by the theoretical $\sum mn$ provides an estimate of the contribution of glucose to the pentose phosphate shunt.

Statistical analysis

Data are presented as mean ± s.d. A two-tailed *t*-test was used for most comparisons, with $P < 0.05$ considered statistically significant.

Supplementary data

Supplementary data are available at *The EMBO Journal* Online (http://www.embojournal.org).

Acknowledgements

Conflict of interest

The authors declare that they have no conflict of interest.

References

Ayyasamy V, Owens KM, Desouki MM, Liang P, Bakin A, Thangaraj K, Buchsbaum DJ, Lobuglio AF, Singh KK (2011) Cellular model of warburg effect identifies tumor promoting function of UCP2 in breast cancer and its suppression by genipin. *PLoS One* **6:** e24792

Baharvand H, Matthaei KI (2003) The ultrastructure of mouse embryonic stem cells. *Reprod Biomed Online* **7:** 330–335

Becker KA, Ghule PN, Therrien JA, Lian JB, Stein JL, van Wijnen AJ, Stein GS (2006) Self-renewal of human embryonic stem cells

is supported by a shortened G1 cell cycle phase. *J Cell Physiol* **209:** 883–893

Boren J, Lee WN, Bassilian S, Centelles JJ, Lim S, Ahmed S, Boros LG, Cascante M (2003) The stable isotope-based dynamic metabolic profile of butyrate-induced HT29 cell differentiation. *J Biol Chem* **278:** 28395–28402

Bouillaud F (2009) UCP2, not a physiologically relevant uncoupler but a glucose sparing switch impacting ROS production and glucose sensing. *Biochim Biophys Acta* **1787:** 377–383

Boyer LA, Lee TI, Cole MF, Johnstone SE, Levine SS, Zucker JP, Guenther MG, Kumar RM, Murray HL, Jenner RG, Gifford DK, Melton DA, Jaenisch R, Young RA (2005) Core transcriptional regulatory circuitry in human embryonic stem cells. *Cell* **122:** 947–956

Brand MD, Affourtit C, Esteves TC, Green K, Lambert AJ, Miwa S, Pakay JL, Parker N (2004a) Mitochondrial superoxide: production, biological effects, and activation of uncoupling proteins. *Free Radic Biol Med* **37:** 755–767

Brand MD, Buckingham JA, Esteves TC, Green K, Lambert AJ, Miwa S, Murphy MP, Pakay JL, Talbot DA, Echtay KS (2004b) Mitochondrial superoxide and aging: uncoupling-protein activity and superoxide production. *Biochem Soc Symp* **71:** 203–213

Brand MD, Esteves TC (2005) Physiological functions of the mitochondrial uncoupling proteins UCP2 and UCP3. *Cell Metab* **2:** 85–93

Buchet K, Godinot C (1998) Functional F1-ATPase essential in maintaining growth and membrane potential of human mitochondrial DNA-depleted rho degrees cells. *J Biol Chem* **273:** 22983–22989

Buzhynskyy N, Sens P, Prima V, Sturgis J, Scheuring S (2007) Rows of ATP synthase dimers in native mitochondrial inner membranes. *Biophys J* **93:** 2870–2876

Cadenas S, Echtay KS, Harper JA, Jekabsons MB, Buckingham JA, Grau E, Abuin A, Chapman H, Clapham JC, Brand MD (2002) The basal proton conductance of skeletal muscle mitochondria from transgenic mice overexpressing or lacking uncoupling protein-3. *J Biol Chem* **277:** 2773–2778

Campanella M, Casswell E, Chong S, Farah Z, Wieckowski MR, Abramov AY, Tinker A, Duchen MR (2008) Regulation of mitochondrial structure and function by the F1Fo-ATPase inhibitor protein, IF1. *Cell Metab* **8:** 13–25

Cao F, Wagner RA, Wilson KD, Xie X, Fu JD, Drukker M, Lee A, Li RA, Gambhir SS, Weissman IL, Robbins RC, Wu JC (2008) Transcriptional and functional profiling of human embryonic stem cell-derived cardiomyocytes. *PLoS One* **3:** e3474

Chan DC, Chen HC, Vermulst M, Wang YE, Chomyn A, Prolla TA, McCaffery JM (2010) Mitochondrial fusion is required for mtDNA stability in skeletal muscle and tolerance of mtDNA mutations. *Cell* **141:** 280–289

Cho YM, Kwon S, Pak YK, Seol HW, Choi YM, Park do J, Park KS, Lee HK (2006) Dynamic changes in mitochondrial biogenesis and antioxidant enzymes during the spontaneous differentiation of human embryonic stem cells. *Biochem Biophys Res Commun* **348:** 1472–1478

Chung S, Arrell DK, Faustino RS, Terzic A, Dzeja PP (2010) Glycolytic network restructuring integral to the energetics of embryonic stem cell cardiac differentiation. *J Mol Cell Cardiol* **48:** 725–734

Considine MJ, Goodman M, Echtay KS, Laloi M, Whelan J, Brand MD, Sweetlove LJ (2003) Superoxide stimulates a proton leak in potato mitochondria that is related to the activity of uncoupling protein. *J Biol Chem* **278:** 22298–22302

Couplan E, del Mar Gonzalez-Barroso M, Alves-Guerra MC, Ricquier D, Goubern M, Bouillaud F (2002) No evidence for a basal, retinoic, or superoxide-induced uncoupling activity of the uncoupling protein 2 present in spleen or lung mitochondria. *J Biol Chem* **277:** 26268–26275

DeBerardinis RJ, Lum JJ, Hatzivassiliou G, Thompson CB (2008) The biology of cancer: metabolic reprogramming fuels cell growth and proliferation. *Cell Metab* **7:** 11–20

Echtay KS, Winkler E, Frischmuth K, Klingenberg M (2001) Uncoupling proteins 2 and 3 are highly active H(+) transporters and highly nucleotide sensitive when activated by coenzyme Q (ubiquinone). *Proc Natl Acad Sci USA* **98:** 1416–1421

Emre Y, Nubel T (2010) Uncoupling protein UCP2: when mitochondrial activity meets immunity. *FEBS Lett* **584:** 1437–1442

Facucho-Oliveira JM, Alderson J, Spikings EC, Egginton S, St John JC (2007) Mitochondrial DNA replication during differentiation of murine embryonic stem cells. *J Cell Sci* **120:** 4025–4034

Figueroa ME, Abdel-Wahab O, Lu C, Ward PS, Patel J, Shih A, Li Y, Bhagwat N, Vasanthakumar A, Fernandez HF, Tallman MS, Sun Z, Wolniak K, Peeters JK, Liu W, Choe SE, Fantin VR, Paietta E, Lowenberg B, Licht JD *et al* (2010) Leukemic IDH1 and IDH2 mutations result in a hypermethylation phenotype, disrupt TET2 function, and impair hematopoietic differentiation. *Cancer Cell* **18:** 553–567

Fischer B, Bavister BD (1993) Oxygen tension in the oviduct and uterus of rhesus monkeys, hamsters and rabbits. *J Reprod Fertil* **99:** 673–679

Frank S, Gaume B, Bergmann-Leitner ES, Leitner WW, Robert EG, Catez F, Smith CL, Youle RJ (2001) The role of dynamin-related protein 1, a mediator of mitochondrial fission, in apoptosis. *Dev Cell* **1:** 515–525

Giraud M, Paumard P, Soubannier V, Vaillier J, Arselin G, Salin B, Schaeffer J, Brèthes D, di Rago J, Velours J (2002) Is there a relationship between the supramolecular organization of the mitochondrial ATP synthase and the formation of cristae? *Biochim Biophys Acta* **1555:** 174–180

Hatefi Y (1985) The mitochondrial electron transport and oxidative phosphorylation system. *Annu Rev Biochem* **54:** 1015–1069

Heytler PG (1979) Uncouplers of oxidative phosphorylation. *Methods Enzymol* **55:** 462–472

Ichikawa N, Chisuwa N, Tanase M, Nakamura M (2005) Mitochondrial ATP synthase residue betaarginine-408, which interacts with the inhibitory site of regulatory protein IF1, is essential for the function of the enzyme. *J Biochem* **138:** 201–207

Jezek P, Borecky J (1998) Mitochondrial uncoupling protein may participate in futile cycling of pyruvate and other monocarboxylates. *Am J Physiol* **275:** C496–C504

Jezek P, Garlid KD (1990) New substrates and competitive inhibitors of the Cl- translocating pathway of the uncoupling protein of brown adipose tissue mitochondria. *J Biol Chem* **265:** 19303–19311

Jezek P, Plecita-Hlavata L, Smolkova K, Rossignol R (2010) Distinctions and similarities of cell bioenergetics and the role of mitochondria in hypoxia, cancer, and embryonic development. *Int J Biochem Cell Biol* **42:** 604–622

Khvorostov I, Zhang J, Teitell M (2008) From MEFs to Matrigel 2: splitting hESCs from MEFs onto Matrigel. *J Vis Exp* **pii:** 831

Klingenberg M, Echtay KS (2001) Uncoupling proteins: the issues from a biochemist point of view. *Biochim Biophys Acta* **1504:** 128–143

Klingenberg M, Huang SG (1999) Structure and function of the uncoupling protein from brown adipose tissue. *Biochim Biophys Acta* **1415:** 271–296

Lee WN, Boros LG, Puigjaner J, Bassilian S, Lim S, Cascante M (1998) Mass isotopomer study of the nonoxidative pathways of the pentose cycle with [1,2-13C2]glucose. *Am J Physiol* **274:** E843–E851

Lee WN, Edmond J, Bassilian S, Morrow JW (1996) Mass isotopomer study of glutamine oxidation and synthesis in primary culture of astrocytes. *Dev Neurosci* **18:** 469–477

Lee WN, Wahjudi PN, Xu J, Go VL (2010) Tracer-based metabolomics: concepts and practices. *Clin Biochem* **43:** 1269–1277

Lin T, Chao C, Saito S, Mazur SJ, Murphy ME, Appella E, Xu Y (2005) p53 induces differentiation of mouse embryonic stem cells by suppressing Nanog expression. *Nat Cell Biol* **7:** 165–171

Lowry WE, Richter L, Yachechko R, Pyle AD, Tchieu J, Sridharan R, Clark AT, Plath K (2008) Generation of human induced pluripotent stem cells from dermal fibroblasts. *Proc Natl Acad Sci USA* **105:** 2883–2888

Maherali N, Ahfeldt T, Rigamonti A, Utikal J, Cowan C, Hochedlinger K (2008) A high-efficiency system for the generation and study of human induced pluripotent stem cells. *Cell Stem Cell* **3:** 340–345

Meshorer E, Misteli T (2006) Chromatin in pluripotent embryonic stem cells and differentiation. *Nat Rev Mol Cell Biol* **7:** 540–546

Minauro-Sanmiguel F, Wilkens S, García JJ (2005) Structure of dimeric mitochondrial ATP synthase: novel F0 bridging features and the structural basis of mitochondrial cristae biogenesis. *Proc Natl Acad Sci USA* **102:** 12356–12358

Morgunov I, Srere PA (1998) Interaction between citrate synthase and malate dehydrogenase. Substrate of oxaloacetate. *J Biol Chem* **273:** 29540–29544

Narendra D, Tanaka A, Suen DF, Youle RJ (2008) Parkin is recruited selectively to impaired mitochondria and promotes their autophagy. *J Cell Biol* **183:** 795–803

Narendra DP, Jin SM, Tanaka A, Suen DF, Gautier CA, Shen J, Cookson MR, Youle RJ (2010) PINK1 is selectively stabilized on impaired mitochondria to activate Parkin. *Plos Biol* **8:** e1000298

Nicholls DG, Lindberg O (1972) Inhibited respiration and ATPase activity of rat liver mitochondria under conditions of matrix condensation. *FEBS Lett* **25:** 61–64

Nicholls DG, Rial E (1999) A history of the first uncoupling protein, UCP1. *J Bioenerg Biomembr* **31:** 399–406

Pan G, Tian S, Nie J, Yang C, Ruotti V, Wei H, Jonsdottir GA, Stewart R, Thomson JA (2007) Whole-genome analysis of histone H3 lysine 4 and lysine 27 methylation in human embryonic stem cells. *Cell Stem Cell* **1:** 299–312

Paumard P, Vaillier J, Coulary B, Schaeffer J, Soubannier V, Mueller D, Brèthes D, di Rago J, Velours J (2002) The ATP synthase is involved in generating mitochondrial cristae morphology. *EMBO J* **21:** 221–230

Pecqueur C, Alves-Guerra C, Ricquier D, Bouillaud F (2009) UCP2, a metabolic sensor coupling glucose oxidation to mitochondrial metabolism? *IUBMB Life* **61:** 762–767

Pecqueur C, Alves-Guerra MC, Gelly C, Levi-Meyrueis C, Couplan E, Collins S, Ricquier D, Bouillaud F, Miroux B (2001) Uncoupling protein 2, *in vivo* distribution, induction upon oxidative stress, and evidence for translational regulation. *J Biol Chem* **276:** 8705–8712

Pecqueur C, Bui T, Gelly C, Hauchard J, Barbot C, Bouillaud F, Ricquier D, Miroux B, Thompson CB (2008) Uncoupling protein-2 controls proliferation by promoting fatty acid oxidation and limiting glycolysis-derived pyruvate utilization. *FASEB J* **22:** 9–18

Prigione A, Fauler B, Lurz R, Lehrach H, Adjaye J (2010) The senescence-related mitochondrial/oxidative stress pathway is repressed in human induced pluripotent stem cells. *Stem Cells* **28:** 721–733

Samudio I, Fiegl M, Andreeff M (2009) Mitochondrial uncoupling and the Warburg effect: molecular basis for the reprogramming of cancer cell metabolism. *Cancer Res* **69:** 2163–2166

Samudio I, Fiegl M, McQueen T, Clise-Dwyer K, Andreeff M (2008) The warburg effect in leukemia-stroma cocultures is mediated by mitochondrial uncoupling associated with uncoupling protein 2 activation. *Cancer Res* **68:** 5198–5205

Saretzki G, Walter T, Atkinson S, Passos JF, Bareth B, Keith WN, Stewart R, Hoare S, Stojkovic M, Armstrong L, von Zglinicki T, Lako M (2008) Downregulation of multiple stress defense mechanisms during differentiation of human embryonic stem cells. *Stem Cells* **26:** 455–464

Sauer H, Rahimi G, Hescheler J, Wartenberg M (2000) Role of reactive oxygen species and phosphatidylinositol 3-kinase in cardiomyocyte differentiation of embryonic stem cells. *FEBS Lett* **476:** 218–223

Sauvanet C, Duvezin-Caubet S, di Rago JP, Rojo M (2010) Energetic requirements and bioenergetic modulation of mitochondrial morphology and dynamics. *Semin Cell Dev Biol* **21:** 558–565

Schieke S, Ma M, Cao L, McCoy JJ, Liu C, Hensel N, Barrett A, Boehm M, Finkel T (2008) Mitochondrial metabolism modulates differentiation and teratoma formation capacity in mouse embryonic stem cells. *J Biol Chem* **283:** 28506–28512

St John JC, Ramalho-Santos J, Gray HL, Petrosko P, Rawe VY, Navara CS, Simerly CR, Schatten GP (2005) The expression of mitochondrial DNA transcription factors during early cardiomyocyte *in vitro* differentiation from human embryonic stem cells. *Clon Stem Cell* **7:** 141–153

Strauss M, Hofhaus G, Schroder RR, Kuhlbrandt W (2008) Dimer ribbons of ATP synthase shape the inner mitochondrial membrane. *EMBO J* **27:** 1154–1160

Sun MG, Williams J, Munoz-Pinedo C, Perkins GA, Brown JM, Ellisman MH, Green DR, Frey TG (2007) Correlated three-dimensional light and electron microscopy reveals transformation of mitochondria during apoptosis. *Nat Cell Biol* **9:** 1057–1065

Vieyra DS, Goodell MA (2007) Pluripotentiality and conditional transgene regulation in human embryonic stem cells expressing insulated tetracycline-ON transactivator. *Stem Cells* **25:** 2559–2566

Watanabe K, Ueno M, Kamiya D, Nishiyama A, Matsumura M, Wataya T, Takahashi JB, Nishikawa S, Nishikawa S, Muguruma K, Sasai Y (2007) A ROCK inhibitor permits survival of dissociated human embryonic stem cells. *Nat Biotechnol* **25:** 681–686

Wu M, Neilson A, Swift AL, Moran R, Tamagnine J, Parslow D, Armistead S, Lemire K, Orrell J, Teich J, Chomicz S, Ferrick DA (2007) Multiparameter metabolic analysis reveals a close link between attenuated mitochondrial bioenergetic function and enhanced glycolysis dependency in human tumor cells. *Am J Physiol Cell Physiol* **292:** C125–C136

Xie H, Valera VA, Merino MJ, Amato AM, Signoretti S, Linehan WM, Sukhatme VP, Seth P (2009) LDH-A inhibition, a therapeutic strategy for treatment of hereditary leiomyomatosis and renal cell cancer. *Mol Cancer Ther* **8:** 626–635

Xu W, Yang H, Liu Y, Yang Y, Wang P, Kim SH, Ito S, Yang C, Xiao MT, Liu LX, Jiang WQ, Liu J, Zhang JY, Wang B, Frye S, Zhang Y, Xu YH, Lei QY, Guan KL, Zhao SM *et al* (2011) Oncometabolite 2-hydroxyglutarate is a competitive inhibitor of alpha-ketoglutarate-dependent dioxygenases. *Cancer Cell* **19:** 17–30

Zhang J, Khvorostov I, Teitell M (2008a) From MEFs to Matrigel 3: passing hESCs from Matrigel onto Matrigel. *J Vis Exp* **pii:** 832

Zhang J, Khvorostov I, Teitell M (2008b) From MEFs to matrigel I: passing hESCs in the presence of MEFs. *J Vis Exp* **pii:** 722